Title:

The relative roles of Modified Circumpolar Deep Water and benthic sources in supplying iron to the recurrent phytoplankton blooms above Pennell and Mawson Banks, Ross Sea, Antarctica.

Author names and affiliations:

Mariko Hatta[1*], Chris I. Measures[1], Phoebe J. Lam[2,3], Daniel C. Ohnemus[2,4], Maureen E. Auro[2], Maxime M. Grand[1,5], Karen E. Selph[1]

[1] School of Ocean and Earth Science and Technology, Department of Oceanography, University of Hawai'i at Manoa, 1000 Pope Road, Honolulu, HI 96822.

[2] Department of Marine Chemistry and Geochemistry, Woods Hole Oceanographic Institution, 266 Woods Hole Road, Woods Hole, MA 02543.

[3] (now at) Department of Ocean Sciences, University of California, Santa Cruz, 1156 High St, Santa Cruz, CA 95064

[4] (now at) Bigelow Laboratory for Ocean Sciences, East Boothbay, ME, USA.

[5] (now at) Ocean and Earth Science, National Oceanography Centre Southampton, University of Southampton Waterfront Campus, European Way, Southampton, SO14 3ZH, UK.

***Corresponding author**

mhatta@hawaii.edu; 1-808-956-6632

Key words (up to 6 key words):

Iron; Banks; Ross Sea; Modified Circumpolar Deep Water; Water mixing; Manganese

Highlights (3-5 highlights, 85 characters, core results):

- Dissolved Fe within the CDW is diluted by mixing with AASW during the formation of MCDW in the Ross Sea.
- MCDW was seen above Mawson Bank but not Pennell Bank.
- A sedimentary input of Fe is seen above Pennell Bank.
- Strong tidal energy over shallow banks brings Fe-rich deep waters to the euphotic zone.
- The presence of MCDW above Mawson Bank hinders mixing of dFe into the euphotic zone.

Abstract: (199 words)

The role that dissolved iron (dFe) rich Circumpolar Deep Water (CDW) might play in sustaining the consistently observed discrete patches of high chlorophyll biomass over Pennell Bank (PB) and Mawson Bank (MB) in the Ross Sea, was investigated during January/February 2011. Over a 26-day period, hydrographic and trace metal clean water sampling was carried out adjacent to both of these banks, in some cases repeatedly. Particulate sampling was also accomplished at selected stations by *in situ* pumping. The results indicate that the dFe content of the CDW is in fact reduced by on-shelf mixing with Antarctic Surface Water as it transitions into modified CDW (MCDW). Our stations above PB, where the maximum bloom is encountered, show no evidence of MCDW presence. In contrast, above MB, where there is a smaller persistent bloom, MCDW was observed. Although both of these stations displayed the imprint of sedimentary Fe input connected to the strong tidal cycles above the banks, the stronger near-bottom density gradient that MCDW produces appears to contribute to reduced vertical mixing of the sedimentary source. Thus, ironically, the presence of MCDW may be hindering the Fe supply to the surface waters, rather than being the source, as originally hypothesized.

1. Introduction

The Southern Ocean is well-known as a High Nutrient Low Chlorophyll (HNLC) region, but within this low biomass area the Ross Sea continental shelf is one of the most productive areas in the Southern Ocean (Sullivan et al., 1993; DiTullio and Smith, 1996; Smith and Gordon, 1997; Arrigo et al., 1998a; Smith and Cosimo, 2008), and thus is considered as an important oceanic CO_2 sink region (Marinov et al., 2005; Arrigo et al., 1998b; Takahashi et al., 2009). The increased biomass seen during iron addition experiments in the Southern Ocean waters (e.g., Martin et al., 1990; Sedwick and DiTullio, 1997) suggests that it is iron, an essential nutrient for phytoplankton growth, that is limiting primary production in the Southern Ocean (Martin et al., 1991; Coale et al., 1996; Sedwick et al., 2000; Boyd, 2002; Coale et al., 2003; 2005; Gerringa et al., 2015; McGillicuddy et al., 2015).

There are multiple potential iron sources to the Ross Sea, such as dust, sea-ice, icebergs, upwelling of deeper waters and sedimentary inputs, etc., and these have been discussed by a variety of authors (Martin et al., 1991; Fitzwater et al., 1996; Sedwick et al., 1996; Sedwick et al., 2000; Measures and Vink, 2001; Boyd, 2002; Coale et al., 2005; Sedwick et al., 2011; Measures et al., 2012; Marsay et al., 2014).

Seasonal iron limitation has been suggested for the Ross Sea as a result of the effects of removal by phytoplankton uptake, particle export, and scavenging (Sedwick and DeTullio, 1997; Sedwick et al., 2000; Coale et al., 2003; 2005; Bertrand et al., 2007). However, in a recent study, Sedwick et al. (2011) reported low dissolved Fe (dFe) concentrations (~0.1 nM) in the euphotic zone of the Ross Sea polynya by late spring (November), concluding that the surface waters in the Ross Sea polynya (southern Ross Sea) can become iron depleted even during an early stage of the seasonal phytoplankton bloom. These authors concluded that in order to sustain the high productivity in the Ross Sea, there must be a significant supply of new dFe to surface waters of the polynya during the growing period.

Satellite ocean colour imagery shows that in contrast to the large areas of high chlorophyll biomass in the inshore regions, the offshore regions show only small patches

of high chlorophyll biomass (Fig. 1). In particular there are discrete blooms that have been occurring above Pennell Bank (PB) and Mawson Bank (MB) at the same time of year from 1998 to 2014 (Reddy and Arrigo, 2006; Kohut et al., this issue). The seasonal persistence of these features also suggests that there should be a continual source of Fe, fuelling phytoplankton blooms above the banks. The dye simulation model of Dinniman et al. (2011) confirmed Circumpolar Deep Water (CDW) intrusions onto the shelf at specific locations primarily determined by the bathymetry (Klinck and Dinniman, 2010), which then mixes with surrounding water masses to become Modified Circumpolar Deep Water (MCDW, Jackobs and Giulivi, 1998; Gordon et al., 2000; Orsi and Wiederwohl, 2009; Whitworth et al., 2013). In addition, Dinniman et al. (2011) showed there was vigorous mixing of the CDW/MCDW with the surface waters in the Ross Sea. Since CDW contains relatively high levels of dFe (~0.5 nM at 65.2°S 174.7°W in the northern Ross Sea, Sedwick et al., 2011; 0.4-0.5 nM, Hoppema et al., 2003; 0.51 ± 0.16 nM, Grand et al., 2015a) compared to summertime surface waters of this shelf region, this water has been considered as a potential source of Fe fuelling primary production in the Ross Sea (Hiscock, 2004; Peloquin and Smith, 2007).

The goal of our research project was to evaluate the role that Fe-enriched CDW may play in fuelling these patches of higher biomass by undertaking a comprehensive physical, chemical, and biological sampling program ("SEAFARERS", Slocum Enhanced Adaptive Fe Algal Research in the Ross Sea, Kohut et al., 2013) around the banks during the late austral summer (Jan 2011), a time when there is no recent seasonal sea ice melt to contribute to the dFe supply. To achieve this, we determined the distributions of dissolved and particulate Fe, dissolved Mn and dissolved Al at key stations on the shelf to enable us to follow the mixing process of CDW as it transitions into MCDW. A key physical process in the Ross Sea is the strong tidal effect in this region and the tide's effect on mixing processes (Robertson et al., 2003; Whitworth and Orsi, 2006; Kohut et al., 2013). To help evaluate these processes our shipboard data gathering included CTD parameters from rosette casts and the ship's acoustic doppler current profiler (ADCP). Additional temperature, salinity, dissolved oxygen, fluorescence and backscatter data were obtained from gliders deployed from the ship, and temperature, salinity, pressure and current meter data were obtained from a mooring

deployed at a station that was occupied multiple times during the cruise (Kohut et al., this issue). Detailed phytoplankton incubation results are presented in earlier manuscripts (Kustka et al., 2015a; 2015b) who also suggested based on their estimates of Fe demand from shipboard incubation experiments and model results that that the recurrent productivity hotspots in the widespread Fe limitation region were supported by the delivery of Fe through vertical exchange processes.

2. Methods

2.1. Sampling

2.1.1 Dissolved trace metal samples

Over 180 water samples were collected for trace metal determinations at 15 stations (Fig. 1) in the Ross Sea between 17 January and 13 February 2011 as part of the SEAFARERS campaign aboard the R/V Nathaniel B. Palmer (cruise NBP 11-01). An additional 12 water samples were collected on 21 February 2011 at station 100 (Fig. 1) at the start of the CLIVAR S4P section (cruise NBP 11-02) that immediately followed the cruise.

Water samples were obtained using a custom-built trace metal (TM) clean rosette consisting of an epoxy painted Al rosette frame containing 12 x 12L GO-FLO bottles (Measures et al., 2008a) and that housed an SBE 911 CTD system which included an SBE 43 dissolved oxygen sensor and a Wet labs FL1 fluorometer. However, because the oxygen sensor froze during the cruise, oxygen data are not available. Immediately after each deployment, the package was recovered, the tops of the GO-FLO bottles were covered with plastic bags and the bottles removed from the frame and carried into a customized 20-foot container van for sub-sampling (Measures et al., 2008a). The GO-FLO bottles were pressurized to 10 psi using 0.2 µm-filtered compressed air and water samples were filtered through 0.45 µm pore size acid washed, 47 mm polysulphone filters (Pall Supor 450 P/N 60173) as they were collected into sample bottles. All sub-sampling was undertaken in the clean van using rigorous trace metal protocols. The sampling system and protocols are described in detail in Measures et al. (2008a). Samples obtained with this system and processed in this manner have been shown during

141 the SAFe inter-comparison cruise (Johnson et al., 2007) and the GEOTRACES inter-
142 calibration cruise to produce concentrations of trace metals (Al, Fe and Mn) that are,
143 within analytical uncertainty, identical to those obtained using other currently accepted
144 sampling methodologies for trace elements (i.e., U.S. GEOTRACES sampling protocols,
145 Cutter and Bruland, 2012). Also, this sampling system has been used successfully to
146 collect uncontaminated trace element samples during several previous projects (e.g.,
147 CLIVAR projects: Measures et al., 2008b; Grand et al., 2014, 2015a, 2015b, 2015c;
148 BWZ project: Measures et al., 2013; Hatta et al., 2013).

149 Filtered seawater samples (0.45 μm pore size) were collected and drawn into acid
150 pre-washed 125 mL polymethylpentene bottles after three rinses with sample water; filled
151 sample bottles were stored in polyethylene bags in the dark at room temperature before
152 the shipboard determination. Duplicate samples were also collected and drawn into
153 previously acid-leached 125 mL HDPE bottles after three sample rinses for shore-based
154 determination of dissolved Fe (dFe) and dissolved Mn (dMn) by Inductively Coupled
155 Plasma Mass Spectrometry (ICP-MS).

156 ***2.1.2 Particulate Fe samples***

157 Size-fractionated suspended particles for particulate Fe determination were
158 collected from 6 depths at selected stations (Stations 14, 55, 70, 35, 24, 7, and 28, shown
159 in Fig. 1) by in-situ filtration using modified dual-flow McLane WTS pumps (Ohnemus
160 and Lam, 2015). Pumps were clamped onto non-metallic Hytrel-jacketed Vectran wire.
161 The filter configurations on the two flowpaths were those used on all US GEOTRACES
162 cruises, and consisted of a 51 μm polyester prefilter followed by paired 0.8 μm
163 polyethersulfone (PES; Pall Supor800) filters "Supor", and a 51 μm polyester prefilter
164 followed by paired quartz fiber filters "QMA" (Whatman QMA) (Cutter et al., 2014;
165 Ohnemus and Lam, 2015). All filters were 142 mm in diameter, and had an active
166 filtering diameter of 126 mm. Up to 478 L and 1100 L were filtered through the "Supor"
167 and "QMA" flowpaths, respectively, over the typical 2-3 hour pump time at an initial
168 pumping rate of 8 L min^{-1}. A complete filter set sandwiched between 1 μm mesh in
169 perforated polypropylene containers was deployed at each station as a "dipped blank",
170 which functioned as a process and adsorption blank.

2.2 Analytical methods

2.2.1 Determination of dissolved trace elements

Dissolved trace element determinations were performed on board ship using the filtered sub-samples from the GO-FLO bottles within a few hours of sample collection. Prior to analysis, samples were acidified to 0.006 M with sub-boiled distilled 6 M HCl, and were then heated in groups of 4 for 3 minutes in a 900 W microwave oven to achieve a temperature of 60 ± 10˚C, to release dFe from complexation in the samples. Samples were allowed to cool to room temperature for at least 1 hour prior to Flow Injection Analysis (FIA). The same method was used in a previous study (Hatta et al., 2015).

Dissolved Al (dAl), dFe and dissolved Mn (dMn) were determined in the filtered, acidified, microwave-treated subsamples using the FIA methods of Resing and Measures (1994) for Al, Measures et al. (1995) for dFe, and Resing and Mottl (1992) for dMn determinations. The limits of detection of the shipboard FIA system, defined during the cruise as three times the standard deviation of replicate analyses of seawater samples of low dFe content, were 0.06 nM for dFe, 0.28 nM for dAl, 0.17 nM for dMn. The analytical precision was 5.5% for dFe at 0.35 nM, 4.5% for dAl at 2.1 nM, 4.4% for dMn at 1.2 nM. However, since most of the results from the shipboard dMn analysis were below the shipboard detection limit, we use the dMn data from the duplicate samples determined using the more sensitive shore-based ICP-MS at the University of Hawaii in this study.

No detectable blank from either the acid or sample buffer were found for the shipboard dAl system. The shipboard dFe system blank, which could not be determined accurately at sea, was estimated post cruise using a subset of replicate samples which were analyzed for dFe using the inductively coupled plasma mass spectrometry (ICP-MS) method of Milne et al. (2010). The shipboard dFe data from each analytical day were corrected using the slope and intercept of a least squares regression between the shore-based ICP-MS and the uncorrected shipboard dFe values from that day (n = 8-12). The magnitude of the correction subtracted from each sample of the uncorrected shipboard FIA dataset (i.e., the shipboard FIA system blank) was 58 ± 35 pM during this

200 cruise, similar to the correction applied to Grand et al. (2015c) dFe dataset, which used
201 the same shipboard FIA manifold during the CLIVAR I05 cruise in the Indian Ocean.

202 Samples for shore-based ICP-MS determinations for dFe and dMn were filtered
203 on board using identical methods as those for the FIA samples, and were stored in 125
204 mL LDPE bottles and acidified in the shore lab to 0.024 M HCl with ultrapure 6N HCl,
205 prior to analysis. Pre-concentration and extraction of samples for the determination of
206 dFe and dMn was performed using a flow injection manifold with an in-line micro-
207 column containing □200 µL of Toyopearl AF Chelate-650 M resin following the
208 protocol of Milne et al. (2010). The pre-concentrated samples were analyzed by ICP-MS
209 (Element2, Thermo Scientific) with an Apex-Q (ESI). Detection limits for Fe and Mn
210 were calculated from 3 standard deviations of determinations of replicate ICP-MS
211 measurements and were approximately 0.01 nmol kg^{-1} and 0.05 nmol kg^{-1}, for Fe and
212 Mn, respectively. Determination of dFe (1.00 ± 0.14 nmol kg^{-1}, n=10) in the
213 GEOTRACES open ocean reference material (GD) was in good agreement with the inter-
214 laboratory averages reported for these materials (GD = 0.95 ± 0.05 nmol kg^{-1}).
215 Determination of dMn (0.23 ± 0.03 nmol kg^{-1}, n=10 (GD); 1.30 ± 0.39 nmol kg^{-1}, n=5
216 (GS)) in the GEOTRACES open ocean reference material were also in good agreement
217 with the inter-laboratory averages reported for these materials (GD = 0.21 ± 0.04 nmol
218 kg^{-1}, GS = 1.45 ± 0.17 nmol kg^{-1}). In this paper, the data presented are from the
219 shipboard FIA Al, the ICP-MS corrected shipboard FIA dFe, and the ICPMS dMn
220 determinations.

221 **2.2.2 Determination of particulate trace metals**

222 Separate subsamples of the top Supor filter (the 0.8 - 51 µm size fraction)
223 representing 3 - 9% of the filter area (median 13 L equivalent volume filtered) were used
224 to determine the total and leachable concentrations of particulate trace metals. Total
225 digestions were effected with the Piranha method (Ohnemus et al., 2014; Ohnemus and
226 Lam, 2015). Briefly, this two-step digestion first uses a strong oxidizing solution (the
227 Piranha reagent: 3 parts concentrated H_2SO_4 to 1 part concentrated H_2O_2) to completely
228 digest the PES filter and other particulate organic material, followed by a strong acid
229 cocktail (4M each of HNO_3, HCl, and HF) to completely digest the silicate components

of suspended marine particles. For acid leachable concentrations of particulate trace metals, separate subsamples were leached in 2 mL 1M HCl at room temperature for 24 hours in 15 mL centrifuge tubes. Samples were centrifuged at 4100 rpm for 45 minutes, and 1.5 mL of supernatant was transferred into a Teflon vial. The cold HCl leach used here is more aggressive than other commonly used weak acid leaches (e.g., Berger et al., 2008), but is similar to weak acid leaches frequently used on size-fractionated in-situ pump samples (Bishop et al., 1977; Lam et al., 2006; Lam and Bishop., 2008), and has the advantage of having been tested on a variety of iron bearing minerals: it has been shown to extract Fe from poorly crystalline Fe(III) oxyhydroxides and a small fraction of some phyllosilicates, but not crystalline Fe(III) oxides (Raiswell et al., 1994).

Total digest and leach solutions were dried down at 110 °C and residues were brought back up into solution with 5% HNO_3. The final solutions were analyzed at the Woods Hole Oceanographic Institution (WHOI) Plasma facility on a Thermo Element2 HR ICP-MS using a quartz spray chamber introduction system. Matrix suppression and internal drift was corrected using 1 ppb In as an internal standard, and concentrations were quantified using mixed element external standard curves (Ohnemus et al., 2014). The detection limit was defined as three times the standard deviation of all dipped blank filters, and was 2.7 nmol $filter^{-1}$ and 9.9 nmol $filter^{-1}$ for leachable and total particulate Fe (L-pFe, T-pFe), respectively. For a median volume filtered of 300 L, this is equivalent to detection limits of 9 pM for L-pFe and 33 pM for T-pFe. Repeat determinations of T-pFe and L-pFe had average relative standard deviations of 3% and 10%, respectively.

2.3 Ancillary data

In order to understand the detailed water column characteristics and biological activity during the cruise, shipboard ADCP, oxygen, photosynthetically active radiation (PAR), and fluorescence data are used in the discussion. However, since there was no PAR sensor or transmissometer sensor attached to the TM rosette and no usable data from the TM rosette oxygen sensor, we use oxygen and PAR data from the regular hydrographic CTD rosette casts, which were deployed within 2-3 hours of the TM casts. Temperature and salinity records indicated that there was no significant change in water properties between these occupations (data not shown).

ADCP data (units: m s^{-1}): In order to identify the surface currents and tidal influence during the sampling period, we use the shipboard hull-mounted ADCP "narrowband" instrument (NB150). These data are publicly available at the website http://currents.soest.hawaii.edu/nbpalmer/ using the cruise recognition code of "nbp1101".

Fluorescence (units: volts): The raw sensor voltages (0-5 volts) from the Wet Labs FLRTD-855 (mounted on the TM rosette during each cast) are used in this study.

Mixed layer depth (units: m): The oceanic mixed layer is defined as the surface layer where the temperature and salinity are vertically homogeneous. In the Southern Ocean, Mixed Layer Depths (MLDs) have previously been defined using criteria based on the change in potential temperature or density with respect to the surface value, (e.g., $\Delta\theta = 0.5°C$, $\Delta\sigma_\theta = 0.125$ kg m^{-3} and $\Delta\theta = 0.2°C$, $\Delta\sigma_\theta = 0.03$ kg m^{-3}). In this study, we define the MLDs using the potential density criteria of $\Delta\sigma_\theta = 0.03$ kg m^{-3} from the surface value, which has also been shown to provide good agreement between density and oxygen based mixed layers in the Bellingshausen Sea (Castro-Morales and Kaiser, 2012). Calculated MLDs (data from regular hydrography CTD rosette and TM rosette) and the depth of the PAR 1% light level are shown in Table 1 together with selected water property parameters within the mixed layer.

3. Results and discussion

Here we report the dissolved (<0.45 μm) Al, Fe, Mn from the trace metal clean rosette sampling system and the particulate (L-pFe and T-pFe) Fe data from the in-situ pumping system. All of the trace metal data presented here are available at the U.S. Antarctic Program Data Center using Entry ID: NBP1101. (http://gcmd.nasa.gov/KeywordSearch/Metadata.do?Portal=GCMD&MetadataView=Full&EntryId=NBP1101).

Potential temperature and salinity data are shown in Fig. 2, with selected stations shown in color in order to identify typical water masses found in the study area. The distribution of hydrographic parameters (temperature, salinity, neutral density, fluorescence, silicate, and phosphate) in the section across the basin (red box shown in

289 Fig. 1) are shown in Fig. 3, and the corresponding dissolved and particulate trace metal
290 distributions are shown in Fig. 4. The vertical depth profiles of hydrographic parameters
291 and trace elements at the repeated sampling station located on the western side of PB in
292 Joides Basin and the offshore station are presented in Fig. 5 and data from the stations
293 above PB and MB are in Fig. 6. Property-property plots of the MCDW (neutral density =
294 28.0 - 28.27 kg m^{-3}) are shown in Fig. 7. Figures were made using Ocean Data View
295 (Schlitzer, 2015). The MLDs at each station are shown in Table 1, and the averaged
296 concentration of each dissolved parameter in the each of the water masses are shown in
297 Table 2. The pFe values (L-pFe and T-pFe) in each water mass are shown in Table 3.

298 **3.1 Water mass characteristics of the Ross Sea**

299 Across the sampling region, the presence of Antarctic Surface Water (AASW),
300 neutral density <28.00 kg m^{-3} (Orsi and Wiederwohl 2009), is evident in the upper 200 m
301 from its high temperature and low salinity. Below 300 m, in the channels between the
302 banks, shelf waters (neutral density >28.27 kg m^{-3}, Orsi and Wiederwohl, 2009) can be
303 seen as High Salinity Shelf Water (HSSW, >34.62) at Stations 2, 24, 55 & 100, and Low
304 Salinity Shelf Water (LSSW, <34.62) at Station 3 (Fig. 2). Between these water masses
305 lay the MCDW, which results from mixing of the inflowing CDW with AASW as it
306 flows southward across the shelf. This MCDW, neutral density 28.00 - 28.27 kg m^{-3}
307 (Orsi and Wiederwohl 2009; Kohut et al., 2013), can be seen along the western side of
308 PB at 218 - 275 m (Stations 16, 24, 41) and along the western side of MB at 150 - 230 m
309 (Station 55). This water mass has a relatively high temperature (-1.3 to -0.6 °C), low
310 salinity (34.52 - 34.55) and low dissolved oxygen (DO; 233 - 250 μmol kg^{-1}, latter not
311 shown in this figure) as a result of the properties of the originating offshore CDW.

312 **3.2 Dissolved and particulate trace metal distributions**

313 The trace element distributions show large contrasts, with low concentrations in
314 surface waters and higher concentrations towards the bottom (Fig. 4). The following
315 sections will focus on each water mass as identified by its physical properties discussed
316 above. We will first look at the characteristics of the two potential mixing partners of

CDW, i.e., the surface waters (AASW) and the deeper waters (HSSW), before using this information to describe the evolution of the MCDW on the shelf.

3.2.1 Surface Waters (AASW) in the mixed layer

Our measured surface dFe values (0.08 - 0.25 nM, Table 2) are similar to the concentrations in surface water found during summer 1995 (0.18 ± 0.08 nM, Sedwick et al., 2000), and are slightly higher than the recently reported results in open polynya surface waters to the south of our study region (0.10 ± 0.05 nM in 2005-2006 summer, 0.06 ± 0.04 nM in 2006 spring, Sedwick et al., 2011; and 0.08 ± 0.07 nM in 2012 summer, Marsay et al., 2014).

Shipboard Fe-addition incubation experiments strongly suggested that all the surface waters of the region were deficient in dFe (Kustka et al., 2015a) at the time of our late summer cruise. However, we observed persistent patches of high fluorescence (i.e., greater phytoplankton blooms), as discussed in the introduction, at Station 35 and over PB at Stations 7, 61 and 28 where fluorometer signals were >0.82 volts. There was also an additional, weaker, patch of high fluorescence at Station 48. These patches corresponded to higher surface temperature, lower silicate and phosphate concentrations (Fig. 3a, e, f), slightly higher dFe values (0.15-0.25 nM) and higher concentrations of L-pFe and T-pFe (Table 3).

In contrast, surface waters with lower fluorescence (<0.4 volts, Stations 55, 70, 16, and 41) had relatively lower dFe values (0.08-0.17 nM). In an Fe-limited region it would be expected, on a steady-state basis, that lower concentrations of dFe would be coincident with higher biomass, since biological uptake would be rapidly removing any biologically available Fe from the dissolved to the particulate phase. However, this is an extremely dynamic region with strong tides and topographically induced mixing, and is thus unlikely to be at steady state. The observation of higher dFe concentrations in places of enhanced biomass is consistent with a location where there is a continuous supply of Fe to surface waters which exceeds the biological removal rate. The vertical profiles of pFe and dFe above PB suggest that there is a potential sedimentary source of L-pFe and dFe, to the upper water column above the banks. We note that at the elevated

346 fluorescence sites, a significant portion of the higher surface pFe is refractory (percent L-
347 pFe <40%). This suggests a sedimentary origin of pFe, which implies a sufficiently
348 vigorous mixing process to supply sedimentary pFe and dFe to surface waters, which we
349 postulate supports the enhanced growth of phytoplankton in these regions. Although
350 localized surface inputs of dFe from patches of melting sea ice cannot be completely
351 ruled out, the archived sea ice concentration satellite imagery (Fig. S1) from
352 Aqua/AMSR-E (https://gcom-w1.jaxa.jp/auth.html) shows that the Ross Sea was ice free
353 from mid December and throughout January/February. Therefore, meltwater dFe inputs
354 are unlikely to be a significant source of dFe when we sampled the region in late January.

355 **3.2.2 Shelf Water and Modified Shelf Waters**

356 At the bottom of the profiles during the outflowing tide (northward flow), we
357 found Shelf Waters (HSSW, neutral density >28.27 kg m^{-3} and temperature <1.85°C,
358 Orsi and Wiederwohl, 2009) at Stations 24 and 100 (Joides Basin, JB), and 55 (DB). In
359 contrast, we did not find these water masses during the incoming (southward flow) when
360 the deepest waters were much warmer and fit the Modified Shelf Water (MSW)
361 definition of neutral density >28.27 kg m^{-3} and temperature >1.85°C (Orsi and
362 Weiderwohl., 2009). Details are shown in Table 2 and Fig. S2. We also found HSSW
363 and LSSW at the inner shelf stations (Stations 2 and 3, Figs. S2 and S3) where are not
364 strongly correlated the out and/or incoming flow (shown in Table 2). At the stations that
365 contain HSSW and LSSW, we see dFe and dMn concentrations continually increasing in
366 the bottom ~100 m towards the deepest sample ~30 m above the sediments. The
367 concentrations of dAl also increased or were higher than 1.5 nM at most of these stations
368 except for Station 3, which interestingly is the only one with LSSW in the deepest water
369 (Fig. S3). Where available, pFe values (both T-pFe and L-pFe) were also high and
370 increased towards the sediments in the deep waters at Stations 55 and 24 (Fig. S3), but
371 those samples were not collected as close to the bottom as the dissolved samples. We
372 take this as evidence of a common benthic source for these dissolved elements probably
373 as a result of the release of pore waters from the sediments (from remineralization) or
374 perhaps by desorption from suspended particles within the benthic nepheloid layer,
375 supported by the strong tidal action on the shelf. This would be similar to the
376 observations reported by Hatta et al. (2013) for the Bransfield Strait region. Additional

support for this idea comes from Marsay et al. (2014), who recently reported a high benthic flux of dFe from the sediments in the southern part of Ross Sea continental shelf during the austral summer 2012.

3.3 Modified Circumpolar Deep Water (MCDW)

In order to understand the evolution of the MCDW as it flows across the shelf, water samples were collected repeatedly at different stages of the tidal cycle at a location in the Joides Basin to the west of PB over an 11-day period (Stations 16, 24, 41, shown in Fig. 1). The dFe profiles during all three occupations show consistent values (0.1 - 0.2 nM) from the surface to 200 m in the AASW (Fig. 5b). Below the AASW is the depth of the core of the MCDW (shown by the coloured star symbol * at each station and defined by a neutral density range of 28.00 - 28.27 kg m^{-3}, Fig. 5). The core of the MCDW, which varies in depth between the occupations as a result of the tidal cycle, is coincident with the depth where Fe concentrations start to increase, but the pattern of increase is different between occupations over the tidal cycle. At Stations 16 and 41, dFe values within the deeper core are 0.27 - 0.33 nM, while at Station 24 (with a shallower MCDW core) dFe values continually increase from 0.27 nM at 220 m to 0.64 nM at the bottom where HSSW is found (>34.62, Fig. 5d). The observed dFe concentration of MCDW in this study (0.22-0.30 nM, Table 2) is similar to the dFe value reported by McGillicuddy et al., (2015) (0.27 ± 0.05 nM). The end-member CDW was sampled at the offshore Station 14, where dFe values range from 0.33 nM at 400 m to 0.42 nM at 1000 m (average 0.36 nM, Table 2). It should be noted that the CDW found here had a maximum potential temperature of 1.3˚C and a salinity of 34.71, indicating that while it is in the fairly broad range of the classical values of CDW (Emery and Meincke, 1986) of 0.1-2˚C and 34.62-34.73 salinity, there may have been local modification of this water mass near the shelf edge (Orsi and Weiderwohl, 2009).

The shipboard ADCP data during the sampling period of each sampling station (~2 hours), along with the mooring data (Kohut et al., 2013), shows the importance of the relative motion of the water across the shelf. There was southward (onshore) flow during the occupation of Stations 16 (-0.32 ± 0.03 m s^{-1}) and 41 (-0.15 ± 0.05 m s^{-1}) and northward (offshore) flow during the occupation of Station 24 (+0.12 ± 0.04 m s^{-1}),

shown in Table 2. These flow patterns suggest that the deep water increase in dFe value at Station 24 is from outflowing HSSW shelf waters, which were enriched from benthic sources further south driven by strong tidal processes. The MSW present at the base of Stations 16 and 41 is much more dilute in dFe, with lower salinity and higher temperatures corresponding to a very small increase in dFe in the bottom-most samples. In contrast, at Station 16, there is a higher dFe value in the MCDW compared to Station 41, which corresponds to stronger onshore flow of the dFe-enriched CDW source (Fig. 5b).

The MCDW is also seen in the deeper channels at Stations 55, 35, 100, 28, the inner shelf at Station 2, and on top of MB at Station 70. As we will argue below, the relative concentration of dFe in the MCDW at these stations appears to be controlled mainly by how much mixing the original CDW has undergone.

We will use water mass properties to examine the origin of the trace metal signals in the MCDW. A property-property plot of salinity and potential temperature (within the neutral density range of MCDW) suggests that MCDW is formed by mixing the CDW end member with a low salinity end member, i.e., ASSW rather than higher salinity HSSW (Fig. 7a). Although Si is not a conservative variable, this inference is supported by the salinity vs. Si plot, which also indicates a low Si, low salinity ASSW source rather than the higher Si, higher salinity HSSW (Fig. 7b). Similarly, the dFe (also not conservative) vs. salinity plot also shows a low dFe mixing partner for the CDW rather than the high dFe HSSW source (Fig. 7c). In addition, the dAl and dMn show this same mixing series, but less clearly (Fig. 7d, e). Thus, the formation of MCDW from CDW results, at this time of year, in a decrease of its dFe content, thus limiting its ability to support biological production. The plot of dFe and dMn in the MCDW (Fig. 7f) also confirms the end member mixing series between the high Fe, low Mn CDW and the low Fe, high Mn AASW. Since the Fe and Mn in the AASW probably have a similar sedimentary source, the fractionation between these two tracers is presumably a result of the shorter residence time of dFe compared to that of dMn in the AASW.

In contrast, the L-pFe values of MCDW (0.93 nM at 230 m at Station 55, and 1.01 nM at 210 m at Station 24, Table 3) are one order of magnitude higher than those in the

CDW (e.g., 0.075 nM at offshore Station 14). Additionally, the T-pFe values of MCDW (2.75 nM at Station 55 and 3.07 nM at Station 24) are one order of magnitude higher than T-pFe in the CDW (0.213 nM at Station 14). This suggests that the MCDW is gaining pFe when it flows onto the shelf, but the dFe is not changing significantly during this process. In contrast, the dMn value of MCDW (0.34 – 0.58 nM) is higher than in the CDW (0.11 nM). The opposite behavior of these two dissolved components is consistent with the MCDW being a mixture between the high Fe, low Mn CDW and a low Fe, high Mn AASW (Fig. 7c, d, f and Table 2). Also, this suggests that this MCDW is probably not mixed with the HSSW that contains the highest dFe values at Station 24 in the trough on the western side of PB.

3.4 The waters above Pennell Bank

Repeat water samples were collected 18 days apart at one station above PB (Stations 7 and 61) and samples were also obtained at Station 48 located to the north of these stations within the same period (Fig. 6). As mentioned before, at Stations 7 and 61, the slightly higher dFe (0.15 nM and 0.25 nM, respectively, shown in Table 2) were seen coincident with higher fluorescence signals (1.73 and 1.66 volts, respectively). In contrast, the lower dFe values (0.13 nM) were seen in the upper 50 m at Station 48 where there was a relatively low fluorescence signal (0.48 volts).

At each of these stations, the dissolved trace element signals are higher below 170 m than in the surface waters, suggesting a benthic input (Fig. 6b, c). We note that all the water above PB is AASW, including the deepest water which has neutral densities (27.99 - 28.03 kg m^{-3}) that are less than, or at the very edge of, the definition of the classic MCDW (28.00 - 28.27 kg m^{-3}) thus the AASW properties are not a result of mixing with CDW/MCDW. Below 170 m, Station 7 shows constant dFe (0.22 ± 0.01 nM) and dMn (0.37 ± 0.03 nM) values, while Station 48 (dFe = 0.22 to 0.27 nM; dMn = 0.50 to 0.70 nM) and Station 61 (dFe = 0.20 to 0.36 nM; dMn = 0.69 to 0.90 nM) show gradual increases from ~170 m to the bottom (Fig. 6b). These features, however, are more pronounced at Station 61 and 48 than at Station 7. Interestingly, shipboard ADCP data during each sampling period (averaged over ~2 hours) shows northward flow (off shelf) during the occupation of Station 7 (+0.14 ± 0.03 m s^{-1}), while there is no strong flow

467 during the occupation of Station 48 (-0.042 ± 0.04 m s^{-1}) and Station 61 (+0.001 ± 0.04 m
468 s^{-1}). Thus, during the occupation of Station 7, under tidal influence, the near-bottom
469 waters were moving northward onto the PB from deeper areas to the south. In contrast,
470 during the occupation of Stations 48 and 61, the tide was fairly slack, i.e., little motion,
471 but prior to the sampling the water had been moving south across the shallow area of
472 Pennell Bank. It thus seems from our profiles that when the bottom waters move south
473 across the shallower parts of the bank, dissolved Fe and Mn are added to the water
474 column. However, when that water moves north onto the bank, it is moving from a
475 neutral density interval that is not in contact with sediments and has not had a significant
476 benthic input before reaching the southern edge of the bank. In addition, the salinity
477 below 150 m at Station 48 is very uniform (Fig. 6d), suggesting that there may be
478 topographically-induced mixing of the bottom waters in this region to the north of the
479 location of Stations 7 and 61. While we do have T-pFe and L-pFe from Station 7
480 showing increases in both loads towards the sediment interface, we do not have
481 equivalent data from Stations 48 and 61. Since there is no presence of MCDW, the
482 elevated Fe seen in the AASW here is not derived from MCDW, but from a local
483 sedimentary input. The increase in dMn values in the bottom waters also suggests a
484 sedimentary input, since MCDW has a lower dMn than AASW.

485 **3.5 The waters above Mawson Bank and comparison to Pennell Bank**

486 In contrast to PB, there is a distinct signal of MCDW at Station 70 above MB
487 between 150 m and the bottom at 255 m (neutral density 28.04 - 28.06 kg m^{-3}). Within
488 this water mass, we see dFe of 0.28 nM (Table 2), similar to that seen at the repeat
489 stations in the Joides Basin along the western side of PB. However, we do not see any
490 increase in dFe at the very bottom of the profile, suggesting either a lack of sedimentary
491 input or its masking by the relatively elevated dFe present in the MCDW (Fig. 6b).
492 Although there appears to be a greater potential supply of dFe in the deeper water column
493 above MB than PB, and a greater potential supply of L-pFe (Fig. 6e), the biomass
494 accumulation is greatest above PB. Given that all of the surface waters of the region are
495 Fe-limited, this suggests that the rate at which these deep supplies of dFe are reaching the
496 euphotic zone must be the factor controlling biological processes in the surface waters.

We note that the bottom layer above MB (Station 70) is more homogenous and isolated from the water column above compared to the bottom layer above PB (Stations 7 and 61), largely the result of stronger tides above MB (Kohut et al., this issue). In fact, calculation of the Brunt Väisälä frequency over MB (Fig. 6f, Fig. S4) reveals a uniform value of <0.8 cycles hr^{-1} in the bottom 80 m layer (from 200 m to the bottom) at MB. Above this bottom layer, there is a sharp increase to 2 cycles hr^{-1}. In contrast, over PB, there is a more gradual increase in buoyancy frequency from 0.5 to 1.8 cycles hr^{-1} in the bottom layer (from 200 m to the bottom). The deep water immediately above PB comprises AASW and has much smaller salinity gradients, so presumably experiences less hindrance to vertical mixing of this putative benthic source. The sharp increase in buoyancy frequency above the more homogeneous bottom layer over MB we take that as evidence that this bottom layer is more isolated from the waters above compared to the bottom layer with a more gradual increase in buoyancy frequency observed over PB. The differences in structure between the bottom layers over each bank, driven by stronger tides over MB, are discussed in Kohut et al. (this issue).

4. Conclusion

Dissolved Fe (dFe) values within MCDW (neutral density of 28.00 - 28.27 kg m^{-3}) to the west of PB during different stages of the tidal cycle show that the dFe content within the CDW is diluted by AASW during its evolution into MCDW.

The bottom waters above PB, with neutral densities of 27.99 - 28.03 kg m^{-3}, are less than or at the very edge of the definition of the classic MCDW. The bottom waters, however, show a sedimentary input of Fe and Mn as a result of tidal mixing and topographic forcing, over the large area of shallow sediments on this bank. This input is more pronounced when the water has flowed across the bank from the north than when it enters from the south.

In contrast, the bottom water above MB (neutral densities of 28.04 -28.06 kg m^{-3}) has a sizeable supply of dFe and pFe associated with the presence of MCDW, but there does not appear to be a sedimentary input into the deep waters here.

525 The fact that there is less biomass in surface waters, but more dFe in deep waters
526 above MB, compared to more biomass in surface waters, but less dFe in deep waters
527 above PB, suggests that there is more limited upward mixing of deep waters above MB
528 (and thus less upward mixing of dFe) as a result of the greater density gradient resulting
529 from salty MCDW in the water column on this bank. Thus, ironically, MCDW may be
530 hindering the supply of Fe to the surface waters, rather than being the source of this
531 limiting micro-nutrient, as originally hypothesized.

532 **Acknowledgements**

533 We thank the Captain and crew of the RV NB Palmer and the RPSC technical
534 support staff both on land and at sea for their professional help in planning and ensuring a
535 successful expedition in Ross Sea. We also thank our fellow scientists for their frequent
536 help in the sub-sampling program and TM casts during the cruise, and the chief scientist
537 Dr. Kohut and co-chief scientist Dr. Kustka and other PIs for making their data available
538 and compiling the cruise data sets. We thank Dr. Swift (chief scientist) and the CLIVAR
539 group for allowing us to occupy an extra station during the following CLIVAR S4P
540 cruise, which had been lost to bad weather, during the SEAFARERS cruise. Finally, we
541 thank the editor Dr. McGillicuddy and two anonymous reviewers and for their fruitful
542 suggestions that helped improve the clarity of this manuscript.

543 We also thank the National Science Foundation for its financial support of this
544 project through Office of Polar Programs Grant numbers ANT-0839024 to CIM and
545 ANT-0838921 to PJL. This is contribution no. XXXX of the School of Ocean Earth
546 Science and Technology, University of Hawaii.

547

548 **References**

549 Arrigo, K.R., A. M. Weiss, and W.O. Smith Jr., 1998a, Physical forcing of phytoplankton
550 dynamics in the southern western Ross Sea, J. Geophys. Res., 103, 1007-1021, DOI:
551 10.1029/97JC02326.

552 Arrigo, K.R., D. Worthen, A.Schnell and M.P. Lizotte, 1998b. Primary production in
553 Southern Ocean waters, J. Geophys. Res., 103, 15587-15600, DOI:
554 10.1029/98JC00930.

555 Berger, C.J.M., Lippiatt, S.M., Lawrence, M.G., Bruland, K.W., 2008. Application of a
556 chemical leach technique for estimating labile particulate aluminum, iron, and
557 manganese in the Columbia River plume and coastal waters off Oregon and
558 Washington. J. Geophys. Res. 113, C00B01. 10.1029/2007jc004703.

559 Bertrand, E. M., M.A. Saito, J. M. Rose, C.R. Riesselman, M.C. Lohan, 2007. A.E.
560 Noble, P.A. Lee, and G.R. DiTullio, Vitamin B12 and iron colimitation of
561 phytoplankton growth in the Ross Sea., Limnol. Oceanogra. , 52, 1079-1093,
562 doi:10.4319/lo.2007.52.3.1079.

563 Bishop, J.K.B., Edmond, J.M., Ketten, D.R., Bacon, M.P., Silker, W.B., 1977. Chemistry,
564 Biology, and Vertical Flux of Particulate Matter from Upper 400 M of Equatorial
565 Atlantic Ocean. Deep-Sea Research 24 (6), 511-548.

566 Boyd, P.W. 2002. Environmental factors controlling phytoplankton processes in the
567 Southern Ocean, J. Phycol., 38. 844-861. Doi:10.1046/j.1529-8817.2002.t01-1-
568 01203.x.

569 Castro-Morales, K., and J. Kaiser., 2012. Using dissolved oxygen concentrations to
570 determine mixed layer depths in the Bellingshausen Sea. Ocean Science **8**, 1-10,
571 doi:10.5194/ox-8-1-2012.

572 Coale, K.H., 1991. Effects of iron, manganese, copper, and zinc enrichments on
573 productivity and biomass in the subarctic Pacific, Limnology and Oceanography 36,
574 1851-1864. DOI: 10.4319/lo.1991.36.8.1851.

575 Coale, K.H., et al.1996. A massive phytoplankton bloom induced by ecosystem-scale
576 iron fertilization experiment in the equatorial Pacific Ocean, Nature,383, 495-501,
577 doi:10.1038/383495a0.

578 Coale, K. H., X. J. Wang, S. J. Tanner, and K. S. Johnson. 2003. Phytoplankton growth
579 and biological response to iron and zinc addition in the Ross Sea and Antarctic
580 Circumpolar Current along 170°W. Deep Sea Research Part II 50:635–653,
581 doi:10.1016/ S0967-0645(02)00588-X.

582 Coale, K. H., R. M. Gordon, and X. Wang. 2005. The distribution and behavior of
583 dissolved and particulate iron and zinc in the Ross Sea and Antarctic circumpolar
584 current along 170°W, Deep Sea Res., Part I. 52, 295-318,
585 doi:10.1016/j.dsr.2005.09.008.

586 Cutter, G.A., Andersson, P., Codispoti, L., Croot, P., Francois, F., Lohan, M.C., Obata,
587 H., Rutgers van der Loeff, M., 2014. Sampling and Sample-handling Protocols for
588 GEOTRACES Cruises, v2.0.
589 http://geotraces.org/images/stories/documents/intercalibration/Cookbook.pdf.

590 Cutter, G., and K. W. Bruland. 2012. Rapid and noncontaminating sampling system for
591 trace elements in global ocean surveys. Limnology and Oceanography: Methods **10**:
592 425–436, doi:10.4319/lom.2012.10.425.

593 Dinniman, M.S., Klinck, J.M., W.O. Smith Jr., 2011. A model study of Circumpolar
594 Deep Water on the West Antarctic Peninsula nad Ross Sea continental shelves.
595 Deep-Sea Research II 58. 1508-1523, doi:10.1016/j.dsr2.2010.11.013.

596 DiTullio, G.R., and W.O. Smith Jr., 1996. Spatial patterns in phytoplankton biomass and
597 pigment distributions in the Ross Sea. J. Geophys. Res.,101. 18467-18477, DOI:
598 10.1029/96JC00034.

599 Emery, W.J., and J. Meincke, 1986. Global water masses: summary and review, Oceanol.
600 acta, 9 (4), 383-391.

601 Fitzwater, S.E., K.S. Johnson, R.M. Gordon, and K.H. Coale, 1996. Iron and zinc in the
602 Ross Sea, 1990 (abstract), Eos Trans. AGU, 76(3), Supplement, AGU-ASLO Ocean
603 Sci. Meet. Suppl., pg. OS192.

Gerringa, L.J.A., P. Laan, G.L. van Dijken, H. van Haren, H.J.W. De Baar, K.R. Arrigo, A.-C. Alderkamp, 2015. Sources of iron in the Ross Sea Polynya in early summer, Marine Chemistry, 177, 447-459, doi:10.1016/j.marchem.2015.06.002.

Gordon, L., I., L.A. Codispoti, J. C. Jennings Jr., F.J. Millero, J.M.Morrison, and C. Sweeney, 2000. Seasonal evolution of hydrographic properties in the Ross Sea, Antarctica, 1996-1997, Deep Sea Res., Part II, 47, 3095-3117, doi:10.1016/S0967-0645(00)00060-6.

Grand, M.M., C.S. Buck, W.M. Landing, C.I. Measures, M. Hatta, W.T. Hiscock, M. Brown, and J.A. Resing. 2014. Quantifying the impact of atmospheric deposition on the biogeochemistry of Fe and Al in the upper ocean: A decade of collaboration with the US CLIVAR-CO2 Repeat Hydrography Program. *Oceanography* 27(1):62–65, http://dx.doi.org/10.5670/oceanog.2014.08.

Grand, M. M., C. I. Measures, M. Hatta, W. T. Hiscock, C. S. Buck, and W. M. Landing (2015a), Dust deposition in the eastern Indian Ocean: The ocean perspective from Antarctica to the Bay of Bengal, Global Biogeochem. Cycles, 29, doi:10.1002/2014GB004898.

Grand, M. M., C. I. Measures, M. Hatta, W. T. Hiscock, W. M. Landing, P. L. Morton, C. S. Buck, P. M. Barrett, and J. A. Resing (2015b), Dissolved Fe and Al in the upper 1000 m of the eastern Indian Ocean: A high-resolution transect along 95°E from the Antarctic margin to the Bay of Bengal, Global Biogeochem. Cycles, 29, doi:10.1002/2014GB004920.

Grand, M.M, C.I. Measures, M. Hatta, P.L. Morton, P. Barrett, A. Milne, J.A. Resing, W.M. Landing (2015c) The impact of circulation and dust deposition in controlling the distributions of dissolved Fe and Al in the south Indian subtropical gyre, Marine Chemistry 176, 110-125. doi: 10.1016/j.marchem.2015.08.002.

630 Hatta, M., Measures, C.I., Selph, K.E., Zhou, M., Hiscock, W.T. 2013. Iron fluxes from
631 the shelf regions near the South Shetland Islands in the Drake Passage during the
632 austral-winter 2006, Deep-Sea Res. II. 90. 89-101.

633 Hatta, M., Measures, C.I., Wu, J., Roshan, S., Fitzsimmons, J.N., Sedwick, P., Morton, P.
634 2015. An overview of dissolved Fe and Mn distributions during the 2010–2011
635 U.S. GEOTRACES north Atlantic cruises: GEOTRACES GA03. Deep Sea Res
636 II. 116, 117-129. doi:19.1916/j.dsr2.2014.07.005.

637 Hiscock, M.R., 2004. The regulation of primary productivity in the Southern Ocean, PhD
638 Dissertation, Duke University, 150pp.

639 Hoppema, M., H. J. W. de Baar, E. Fahrbach, H. H. Hellmer, and B. Klein (2003),
640 Substantial advective iron loss diminishes phytoplankton production in the
641 Antarctic Zone, Global Biogeochem. Cycles, 17(1), 1025,
642 doi:10.1029/2002GB001957.

643 Jackobs, S.A., and C.F.Giulivi, Interannual ocean and sea ice variability in the Ross Sea.
644 1998. In Ocean, Ice, and atmosphere: Interactions at the Antarctic Continental
645 Margin, edited by S.S. Jacovs, and R.F. Weiss, pp. 135-150, AGU.
646 DOI: 10.1029/AR075p0135.

647 Johnson, K. S., et al. (2007), Developing standards for dissolved iron in seawater, Eos
648 Trans. AGU, 88(11), 131–132, doi:10.1029/2007EO110003.

649 Klinck, J. M., and M. S. Dinniman, 2010. Exchange across the shelf break at high
650 surthern latitudes, Ocean Sci., 6(2), 513-524. Doi:10.5194/os-6-513-2010.

651 Kohut, J., E. Hunter, and B. Huber. 2013. Small-scale variability of the cross-shelf flow
652 over the outer shelf of the Ross Sea, J. Geophys. Res. Oceans, 118, 1863–1876,
653 doi:10.1002/jgrc.20090.

654 Kohut, J.T., Kustka, A.B., Hiscock, M., Lam, P., Measures, C.I., Milligan, Al., White, A.,
655 Auro, M.E., Carvalho, F., Hatta, M., Jones, B., Ohnemus, D.C., and Swarts, J.M.
656 Mesoscale variability of the summer bloom over the Northern Ross Sea Shelf: A
657 Tale of two Banks. Journal of Marine Systems (this issue).

Kustka, A., Jones, B.M., Hatta, M., Field, M. P., and A. J. Milligan, 2015a. The influence of iron and siderophores on eukaryotic phytoplankton growth rates and community composition in the Ross Sea, Marine Chemistry. 173. 195-207. doi:10.1016/j.marchem.2014.12.002.

Kustka, A.B., J.T. Kohut, A.E. White, P.J. Lam, A.J. Milligan, M.S. Dinniman, S. Mack, E. Hunter, M.R. Hiscock, W.O. Smith Jr, and C.I. Measure, 2015b. The roles of MCDW and deep water iron supply in sustaining a recurrent phytoplankton bloom on central Pennell Bank (Ross Sea). Deep Sea Research Part I. 105: p. 171-185.

Lam, P.J., Bishop, J.K.B., 2008. The continental margin is a key source of iron to the HNLC North Pacific Ocean. Geophysical Research Letters 35, L07608. doi:10.1029/2008GL033294.

Lam, P.J., Bishop, J.K.B., Henning, C.C., Marcus, M.A., Waychunas, G.A., Fung, I.Y., 2006. Wintertime phytoplankton bloom in the subarctic Pacific supported by continental margin iron. Global Biogeochemical Cycles 20 (1), doi:10.1029/2005GB002557.

Marinov, I., A. Gnanadesikan, J.R., Toggweiler, and J. L. Sarmiento, 2005. The Southern Ocean biogeochemical divide, Nature, 441, 964-967, doi:10.1038/natur04883.

Marsay, C.M., P.N. Sedwick, M.S. Dinniman, P.M. Barrett, S.L., Mack, and D.J. McGillicuddy Jr. (2014), Estimating the benthic efflux of dissolved iron on the Ross Sea continental shelf, Geophys. Res. Lett, 41, 7576-7583, doi:10.1002/2014GL061684.

Martin, J.H., 1990. Glacial–interglacial CO_2 change: the iron hypothesis. Paleocea-nography 5 (1), 1–13, 10.1029/PA005i001p00001.

Martin, J.H., R.M. Gordon, and S.E. Fitzwater, 1991. The case for iron, Limnol. Oceanography 36(8), 1793-1802.

McGillicuddy, D.J., P.N. Sedwick, M.S. Dinniman, K.R. Arrigo, T.S. Bibby, B.J.W. Greenan, E.E Hofmann, J.M. Klinck, W.O. Smith Jr., S.L. Mack, C.M. Marsay, B.M. Sohst and G.L. can Dijken, 2015. Iron supply and demand in an Antarctic shelf ecosystem. Geophys. Res. Lett. 42, 8088-8097, doi:10.1002/2015GL065727.

Measures, C.I., J. Yang, and J.A. Resing, J., 1995. Determination of iron in seawater by flow injection analysis using in-line preconcentration and spectrophotometric detection, Mar. Chem., **50**, 3-12.

Measures, C.I., Vink, S., 2001. Dissolved Fe in the upper waters of the Pacific sector of the Southern Ocean. Deep-Sea Res. II 48, 3913–3941, doi:10.1016/S0967-0645(01)00074-1.

Measures, C. I., W. M. Landing, M. T. Brown, and C. S. Buck (2008a) A commercially available rosette system for trace metal clean sampling, *Limnol. Oceanogr. Methods* **6**:384-394. doi: 10.4319/lom.2008.6.384.

Measures, C. I., W. M. Landing, M. T. Brown, and C. S. Buck (2008b), High-resolution Al and Fe data from the Atlantic Ocean CLIVAR-CO2 Repeat Hydrography A16N transect: Extensive linkages between atmospheric dust and upper ocean geochemistry, Global Biogeochem. Cycles, 22, GB1005, doi:10.1029/2007GB003042.

Measures, C.I., M. Hatta, and M.M. Grand. 2012. Bioactive trace metal distributions and biogeochemical controls in the Southern Ocean. *Oceanography* 25(3):122–133, http:// dx.doi.org/10.5670/oceanog.2012.85.

Measures, C.I., Brown, M.T., Selph, K.E., Apprill, A., Zhou, M., Hatta, M., Hiscock, W.T. 2013. The Influence of Shelf Processes in Delivering Dissolved Iron to the HNLC waters of the Drake Passage, Antarctica, Deep-Sea Res. II. 90. 77-88, doi: 10.1016/j.dsr2.2012.11.004.

Milne, A., W.Landing, M.Bizimis, P. Morton, 2010. Determination of Mn, Fe, Co, Ni, Cu, Zn, Cd and Pb in seawter using high resolution magnetic sector inductively

712 coupled mass spectrometry (HR-ICP-MS). Analytica Chimica Acta 665, 200-207.
713 doi:10.1016/j.aca.2010.03.027.

714 Ohnemus, D.C., Auro, M.E., Sherrell, R.M., Lagerstrom, M., Morton, P.L., Twining,
715 B.S., Rauschenberg, S., Lam, P.J., 2014. Laboratory intercomparison of marine
716 particulate digestions including Piranha: a novel chemical method for dissolution
717 of polyethersulfone filters. Limnology and Oceanography-Methods 12, 530-547.
718 10.4319/lom.2014.12.530.

719 Ohnemus, D.C., Lam, P.J., 2015. Cycling of lithogenic marine particles in the US
720 GEOTRACES North Atlantic transect. Deep Sea Research Part II: Topical
721 Studies in Oceanography 116, 283-302, DOI:10.1016/j.dsr2.2014.11.019.

722 Orsi, A. H., and C.L. Wiederwohl. 2009. A recount of Ross Sea waters. Deep-Sea Res. II.
723 56. 778-795. doi:10.1016/j.dsr2.2008.10.033.

724 Peloquin, J.A., Smith Jr., W.O., 2007. Phytoplankton blooms in the Ross Sea, Antarctica:
725 interannual variability in magnitude, temporal patterns, and composition. Journal
726 of Geophysical Research 112, C08013. doi:10.1029/ 2006JC003816.

727 Raiswell, R., Canfield, D.E., Berner, R.A., 1994. A comparison of iron extraction
728 methods for the determination of degree of pyritisation and the recognition of
729 iron-limited pyrite formation. Chemical Geology 111 (1-4), 101-110.

730 Reddy, T. E., and K. R. Arrigo, 2006. Constraints on the extent of the Ross Sea
731 phytoplankton bloom, J. Geophys. Res., 111, C07005,
732 doi:10.1029/2005JC003339.

733 Resing, J. and C.I. Measures. 1994. Fluorimetric determination of Al in seawater by FIA
734 with in-line preconcentration, Anal. Chem., 66,4105-4111.

735 Resing, J. A. and M. J. Mottl. 1992. Determination of Manganese in seawater using flow
736 injection analysis with on-line preconcentration and spectrophotometric,
737 Analytical Chemistry, **64**, 2682-2687.

738 Robertson, R., Beckmann, A., H. Hellmer. 2003. M_2 tidal dynamics in the Ross Sea.
739 Antarctic Science 15. 41-46. doi:10.1017/S0954102003001044.

740 Schlitzer, R., Ocean Data View, http://odv.awi.de, 2015.

741 Sedwick P. N., G. DiTullio, and D.Mackey, 1996. Dissolved iron and manganese in
742 surface waters of the Ross Sea, austral summer 1995-1996, Antarctic journal of
743 the United States / v.31 no.2. 1996, pp.128-130.

744 Sedwick, P. N., and G.R. DiTullio, 1997. Regulation of algal blooms in Antarctic shelf
745 waters by the release of iron from melting sea ice, Geophys. Res. Lett., 24, 2515-
746 2518, 10.1029/97GL02596.

747 Sedwick, P.N., G.R. DiTullio, D.J. Mackey. 2000. Iron and manganese in the Ross Sea,
748 Antarctica: Seasonal iron limitation in Antarctic shelf waters. Journal of
749 geophysical research, 105. C5. 11321-11336, doi:10.1029/2000JC000256.

750 Sedwick, P. N., C.M. Marsay, B.M. Sohst, A.M. Aguilar-Islas, M.C. Lohan, M.C. Long,
751 K.R. Arrigo, R.B. Dunbar, M.A. Saito, W.O. Smith, G.R. DiTullio, 2011. Early
752 season depletion of dissolved iron in the Ross Sea polynya: Implications for iron
753 dynamics on the Antarctic continental shelf, J. Geophys. Res., 116, C12019,
754 doi:10.1029/2010JC006553.

755 Smith Jr., W.O. and J.C. Comiso, 2008. Influence of sea ice on primary production in the
756 Southern Ocean: a satellite perspective. Journal of Geophysical Research 113,
757 C05S93. doi:10.1029/2007JC004251.

758 Smith W.O., Jr. and L.I. Gordon, 1997. Hyperproductivity of the Ross Sea (Antarctica)
759 polynya during austral spring, Geophys. Res. Lett., 24, 233-236, DOI:
760 10.1029/96GL03926.

761 Sunda W.G. and S.A. Huntsman, 1986. Relationships among growth rate, cellular
762 manganese concentrations and manganese transport kinetics in estuarine and
763 oceanic species of the diatom Thalassiosira, J. Phyco., 22. 259-270.
764 DOI: 10.1111/j.1529-8817.1986.tb00022.x.

765 Sunda, W.G., Huntsman, S.A., 1995. Iron uptake and growth limitation in oceanic and
766 coastal phytoplankton. Mar. Chem. 50, 189–206, doi:10.1016/0304-
767 4203(95)00035-P.

768 Sullivan, C.W., K.R. Arrigo, C.R., McClain, J.C. Comiso, and J. Firestone, 1993.
769 Distributions of phytoplankton blooms in the Southern Ocean, Science 262
770 (5141):1832-7.

771 Takahashi T., Sutherland, S. C., Wanninkhof, R., Sweeney, C., Feely, R.A., Chipman, D.
772 W., Hales, B., Friederich, G., Chavez, F., Sabine, C., Watson, A., Bakker, D. C.
773 E., Schuster, U., Metzl, N., Yoshikawa-Inoue, H., Ishii, M., Midorikawa, T.,
774 Nojiri, Y., Körtzinger, A., Steinhoff, T., Hoppema, M., Olafsson, J., Arnarson, T.
775 S., Tilbrook, B., Johannessen, T., Olsen, A., Bellerby, R., Wong, C. S., Delille, B.
776 D., Bates, N. R., and H.J.W. de Baar, 2009. Climatological mean and decadal
777 change in surface ocean pCO_2, and net sea–air CO_2 flux over the global oceans,
778 Deep Sea Research Part I: 56, Issue 11, 2075-2076, DOI:
779 10.1016/j.dsr2.2008.12.009.

780 Whitworth III, T., and A.H. Orsi. 2006. Antarctic Bottom Water production and export
781 by tides in the Ross Sea. Geophysical Res Lett. 33. L12609.
782 doi:10.1029/2006GL026357.

783 Whitworth III, T., A. H. Orsi, S.-J. Kim, W.D. J. Nowlin, and R.A. Locarnini. 2013.
784 Water masses and mixingnear the Antarctic Slope Front, Ocean, Ice and Antarct.
785 Res. Ser., 75, 1-29, DOI: 10.1029/AR075p0001.

786

Figures and Tables

Figure 1. Map of sampling stations in the Ross Sea during the 2011 SEAFARERS cruise and a sampling station (Station 100) during the subsequent CLIVAR S4P cruise. The sampling stations are shown with blue circles, adjacent to the station numbers. The red box encompasses the stations that comprise a section across Drygalsky Basin (DB), Mawson Bank (MB), Joides Basin (JB), Pennell Bank (PB), and Glomar Challenger Basin (GCB). The insert (top left) shows a composite satellite image of Chl-*a* from MODIS during this expedition (blue is lower values and red is higher values of Chl-*a* fluorescence).

Figure 2. Potential temperature and salinity data from all water sampling depths at stations occupied, with selected stations shown in color in order to identify the typical water masses found. Offshore station (Station 14, red circles), one station at the western side of Pennell Bank (Station 16, green squares), the inner shelf with MCDW water (Station 2, blue cross), and inner shelf (Station 3, black circles) with less pronounced MCDW features. Station 48 (purple circles) is located above Pennell Bank. Abbreviations: AASW = Antarctic Surface Water (neutral density <28.00 kg m^{-3}); CDW = Circumpolar Deep Water (neutral density 28.00-28.27 kg m^{-3}); MCDW = Modified Circumpolar Deep Water (neutral density 28.00-28.27 kg m^{-3}); MSW = Modified Shelf Water (neutral density >28.27 kg m^{-3} and potential temperature θ > -1.85 °C); LSSW = Low Salinity Shelf Water (neutral density >28.27 kg m^{-3}, potential temperature θ < -1.85 °C, and Salinity <34.62); HSSW = High Salinity Shelf Water (neutral density >28.27 kg m^{-3}, potential temperature θ < -1.85 °C, and Salinity >34.62). The water masses were defined by Orsi and Weiderwohl (2009).

Figure 3. Distributions of water properties in the section above Pennell and Mawson Banks (stations shown in Fig. 1) as a function of longitude. (a) Temperature (°C), (b) Salinity, (c) Neutral Density (kg m^{-3}), (d) Fluorescence (volts), (e) Silicate (μM), and (f) Phosphate (μM). Averaged values are shown at the stations (16/24/41 and 7/61) that were occupied repeatedly.

Figure 4. Distributions of trace elements in the section above Pennell and Mawson Banks (stations shown in Fig. 1) as a function of longitude. (a) L-pFe (nM), (b) T-pFe (nM), (c) Percent L-pFe (%), (d) dissolved Al (dAl, nM), (e) dissolved Mn (dMn, nM), and (f) dissolved Fe (dFe, nM). Averaged values are shown at the stations (16/24/41 and 7/61) that were occupied repeatedly.

Figure 5. Vertical depth (m) profiles of various parameters from the repeated stations on the western side of Pennell Bank (Stations 16, 24, and 41) and the offshore station (Station 14). (a) temperature (°C), (b) dissolved Fe (dFe, nM), (c) dissolved Mn (dMn, nM), (d) salinity, (e) L-pFe (nM), (f) T-pFe (nM). The depth of the core of the MCDW is shown by the star (*) symbol, in a color matching that of the corresponding profile.

Figure 6. The vertical depth (m) profiles of parameters from the repeated stations at the top of Pennell Bank (Stations 7, 61, and 48). (a) temperature (°C), (b) dissolved Fe (dFe, nM), (c) dissolved Mn (dMn, nM), (d) salinity, (e) L-pFe (nM), (f) Brunt-Väisälä Frequency (cycles h^{-1}).

Figure 7. Property-property plots (various properties vs. Salinity and dFe vs. dMn) of the MCDW and CDW (neutral density = 28.00 - 28.27 kg m^{-3}), at the repeated stations along the western side of Pennell Bank (Stations 16, 24, 41; all MCDW stations), the inshore station (Station 3) that is less modified with MCDW water, and the offshore station (Station 14, CDW station). Each of the following is plotted as a function of salinity: (a) potential temperature (water mass abbreviations as in Fig. 2), (b) silicate (μM), (c) dFe (nM), (d) dMn (nM), and (e) dAl (nM). Finally, (f) dFe is plotted as a function of dMn for the MCDW stations.

Table 1. Station locations (refer to Fig. 1), and Mixed Layer Depth (MLD, db), maximum fluorescence depth (Max. FL depth, m), and the depth of 1% PAR. The MLD and 1% PAR depth from the hydrographic rosette are indicated with a "*" in their column headers.

Table 2. Station water mass characteristics. Shown are station locations, averaged dFe and dMn (nM), fluorescence signals (FL, volts), and the density ranges for each water mass. A question mark in the Water Mass column indicates that the identity of the water

844 masses is not clear from the available data. Abbreviations: AASW = Antarctic Surface
845 Water; CDW = Circumpolar Deep Water; MCDW = Modified Circumpolar Deep Water;
846 MSW = Modified Shelf Water; SW= Shelf Water; MB = Mawson Bank; PB = Pennell
847 Bank, DB = Drygalsky Basin; JB = Joides Basin; GCB = Glomar Challenger Basin. The
848 values with the (*) symbol are the average values within the defined density range.

849 **Table 3**. The leachable and total pFe concentrations (L-pFe and T-pFe, respectively, nM)
850 in the water masses at stations occupied in the Ross Sea, with the station regions
851 indicated. Abbreviations: AASW = Antarctic Surface Water; CDW = Circumpolar Deep
852 Water; MCDW = Modified Circumpolar Deep Water; MSW = Modified Shelf Water;
853 SW= Shelf Water; MB = Mawson Bank; PB = Pennell Bank, DB = Drygalsky Basin; JB
854 = Joides Basin; GCB = Glomar Challenger Basin.

855 Supplemental figures

856 Fig. S1. The sea ice concentration satellite imagery from Aqua/AMSR-E (https://gcom-
857 w1.jaxa.jp/auth.html) from Dec 2010 to Feb 2011, along with our relevant station
858 locations Station 7 was sampled on Jan 22, and Station 61 was on Feb 9, and Station 70
859 was on Feb 10.

860 Fig. S2. Vertical depth (m) profiles of various parameters at the stations characterized as
861 shelf water (top panels) and modified shelf water (bottom panels). Panel
862 shows temperature (°C) in (a) and (d), salinity in (b) and (e), and neutral density (kg m^{-3})
863 in (c) and (f). Abbreviations: LSSW = Low Salinity Shelf Water (neutral density >28.27
864 kg m^{-3}, potential temperature θ < -1.85 °C, and Salinity <34.62); HSSW = High Salinity
865 Shelf Water (neutral density >28.27 kg m^{-3}, potential temperature θ < -1.85 °C, and
866 Salinity >34.62). Water masses as defined by Orsi and Weiderwohl (2009).

867 Fig. S3. Vertical depth (m) profiles of various parameters at the inner shelf stations
868 (Stations 2 and 3), Stations 24 and 100 (JB), and Station 55 (DB). Panel (a) temperature
869 (°C), (b) salinity, (c) dissolved Fe (nM), (d) dissolved Mn (nM), (e) dissolved Al (nM),
870 and (f) T-pFe (nM). Bottom depth (m) of the each station is shown as a brown line.
871 Abbreviations: LSSW = Low Salinity Shelf Water (neutral density >28.27 kg m^{-3},
872 potential temperature θ < -1.85 °C, and salinity <34.62); HSSW = High Salinity Shelf

873 Water (neutral density >28.27 kg m^{-3}, potential temperature θ < -1.85 °C, and salinity
874 >34.62). Water masses as defined by Orsi and Weiderwohl (2009).

875 Fig. S4. Vertical depth (m) profiles of parameters from the repeated stations at the top of
876 Pennell Bank (Stations 7 and 61) and the top of Mawson Bank (Station 70). (a)
877 temperature (°C), (b) salinity, (c) potential density anomaly (kg m^{-3}), (d) Brunt-Väisälä
878 Frequency (cycles h^{-1}).

879

880 **Table 1.** Station locations (refer to Fig. 1), and Mixed Layer Depth (MLD, db), maximum fluorescence depth (Max. FL depth, m), and
881 the depth of 1% PAR. The MLD and 1% PAR depth from the hydrographic rosette are indicated with a "*" in their column headers.

882

Location	Station #	Longitude	Latitude	MLDs [db]	Max. fluorescence depth [m]	MLDs*	1% PAR depth [m]*
Offshore	14	178.00	-74.50	40.00	10-46	28	43
Offshore	30	178.75	-74.20	19.00	20-50	22	24
DB	55	173.17	-73.08	74.00	0-74	55	50
above MB	70	174.00	-73.35	49.00	60-90	43	65
JB	35	174.83	-73.58	33.00	24-48	33	36
JB	100	175.83	-73.88	40.00	20-70	No data	No data
JB	16	176.67	-74.13	32.00	62-104	31	82
JB	24	176.66	-74.14	25.00	23-58	14	58
JB	41	176.67	-74.13	38.00	21-40	37	66
above PB	7	178.00	-74.50	30.00	22-47	41	22
above PB	61	178.00	-74.50	40.00	10-46	51	23
above PB	48	178.75	-74.20	40.00	49-61	19	61
GBC	28	179.50	-74.87	44.00	10-44	40	28
Inner shelf	2	174.00	-75.19	43.00	33-60	32	No data
Inner shelf	3	178.52	-76.16	44.00	10-45	40	54
Inner shelf	21	177.00	-75.75	39.00	10-30	44	24

883

884

885 **Table 2.** Station water mass characteristics. Shown are station locations, averaged dFe and dMn (nM), fluorescence signals (FL,
886 volts), and the density ranges for each water mass. A question mark in the Water Mass column indicates that the identity of the water
887 masses is not clear from the available data. Abbreviations: AASW = Antarctic Surface Water; CDW = Circumpolar Deep Water;
888 MCDW = Modified Circumpolar Deep Water; MSW = Modified Shelf Water; SW= Shelf Water; MB = Mawson Bank; PB = Pennell
889 Bank, DB = Drygalsky Basin; JB = Joides Basin; GCB = Glomar Challenger Basin. The values with the (*) symbol are the average
890 values within the defined density range.

Water mass	Region	Station #	dFe (nM)	dMn (nM)	fluorescence (volts)	neutral density range, water mass, ADCP flow rate within 2-3 hours during the sampling period (N=Northward flow, S=Southward flow)
AASW within mixed layer	Offshore	14	0.16	0.24	0.39	
	DB	55	0.08*	0.45*	0.39*	
	above MB	70	0.16*	0.35*	0.37*	
	JB	35	0.18	0.08	0.92	
	JB	100	0.20	0.11	0.57	
	JB	16	0.17	0.1	0.31	
	JB	24	0.19	0.17	0.81	
	JB	41	0.11	0.36	0.4	
	above PB	48	0.13*	0.17*	0.48*	
	above PB	7	0.15*	0.05*	1.73*	

	above PB	61	0.25	<0.05	1.66	
	GCB	28	0.16	0.05	1.42	
	Inner shelf	2	0.13*	0.35*	0.4*	
	Inner shelf	3	0.19*	0.13*	0.51*	
	Inner shelf	21	0.18*	0.09*	1.46*	
CDW	Offshore	14	0.36*	0.11*		28.00-28.27
MCDW	DB	55	0.26*	0.37*		28.02-28.12
	above MB	70	0.28*	0.37*		28.03-28.08
	JB	35	0.26*	0.54*		28.03-28.08
	JB	100	0.26*	0.42*		28.03-28.08
	JB	16	0.30*	0.34*		28.03-28.20
	JB	24	0.22*	0.49*		28.05-28.19
	JB	41	0.24*	0.46*		28.03-28.14
	above PB	61	0.28*	0.74*		28.00-28.03
	above PB	48	0.24*	0.53*		27.99
	above PB	7	0.23*	0.37*		28.00-28.03
MCDW	GCB	28	0.22*	0.39*		28.00-28.15
MCDW	Inner Shelf	2	0.26*	0.58*		28.04-28.10
	Inner Shelf	3	0.21*	0.73*		28.00-28.06
	Inner Shelf	21	0.31*	0.51*		28.01-28.06
MSW&SW	DB	55	0.25-0.53	0.44-0.65		>28.27, HSSW, N +0.02±0.10 meter sec^{-1}
	JB	35	0.38-0.40	0.47-0.50		>28.27, MSW, S -0.09±0.06 meter sec^{-1}
	JB	100	0.25-0.56	0.34-0.79		>28.27, HSSW
	JB	16	0.28-0.35	0.32-0.44		>28.27, MSW, S

						-0.32±0.03 meter sec^{-1}
	JB	24	0.33-0.64	0.40-0.89		>28.27, HSSW, N +0.12±0.04 meter sec^{-1}
	JB	41	0.25-0.36	0.43-0.78		>28.27, MSW, S -0.15±0.05 meter sec^{-1}
	GBC	28	0.28-0.47	0.44-0.88		>28.27, MSW, N +0.09±0.03 meter sec^{-1}
	Inner shelf	2	0.35-0.76	0.78-1.44		>28.27, HSSW, S -0.05±0.04 meter sec^{-1}
	Inner shelf	3	0.22-0.73	0.78-2.17		>28.27, LSSW, N +0.13±0.03 meter sec^{-1}
	Inner Shelf	21	0.30-0.37	0.42-1.12		>28.27, MSW, N +0.12±0.03 meter sec^{-1}

891

892

893 **Table 3.** Leachable and total pFe concentrations (L-pFe and T-pFe, respectively, nM) in the water masses at stations occupied in the
894 Ross Sea, with the station regions indicated. Abbreviations: AASW = Antarctic Surface Water; CDW = Circumpolar Deep Water;
895 MCDW = Modified Circumpolar Deep Water; MSW = Modified Shelf Water; SW= Shelf Water; MB = Mawson Bank; PB = Pennell
896 Bank, DB = Drygalsky Basin; JB = Joides Basin; GCB = Glomar Challenger Basin.

Water mass	Region	Station #	L-pFe (nM)	T-pFe (nM)
AASW	offshore	14	0.079	0.169
	DB	55	0.073	0.166
	above MB	70	0.054	0.095
	JB	35	0.045	0.053
	JB	24	0.042	0.047
	above PB	7	0.12	0.313
	GCB	28	0.101	0.387
CDW	offshore	14	0.075	0.213
MCDW	DB	55	0.93	2.75
	above NB	70	0.99	3.35
	JB	24	1.01	3.07
	above PB	7	0.72	2.76
MSW & SW	DB	55	2.68	8.03
	JB	35	2.28	8.76
	JB	24	2.15	6.84

897

Figure 1

Click here to download high resolution image

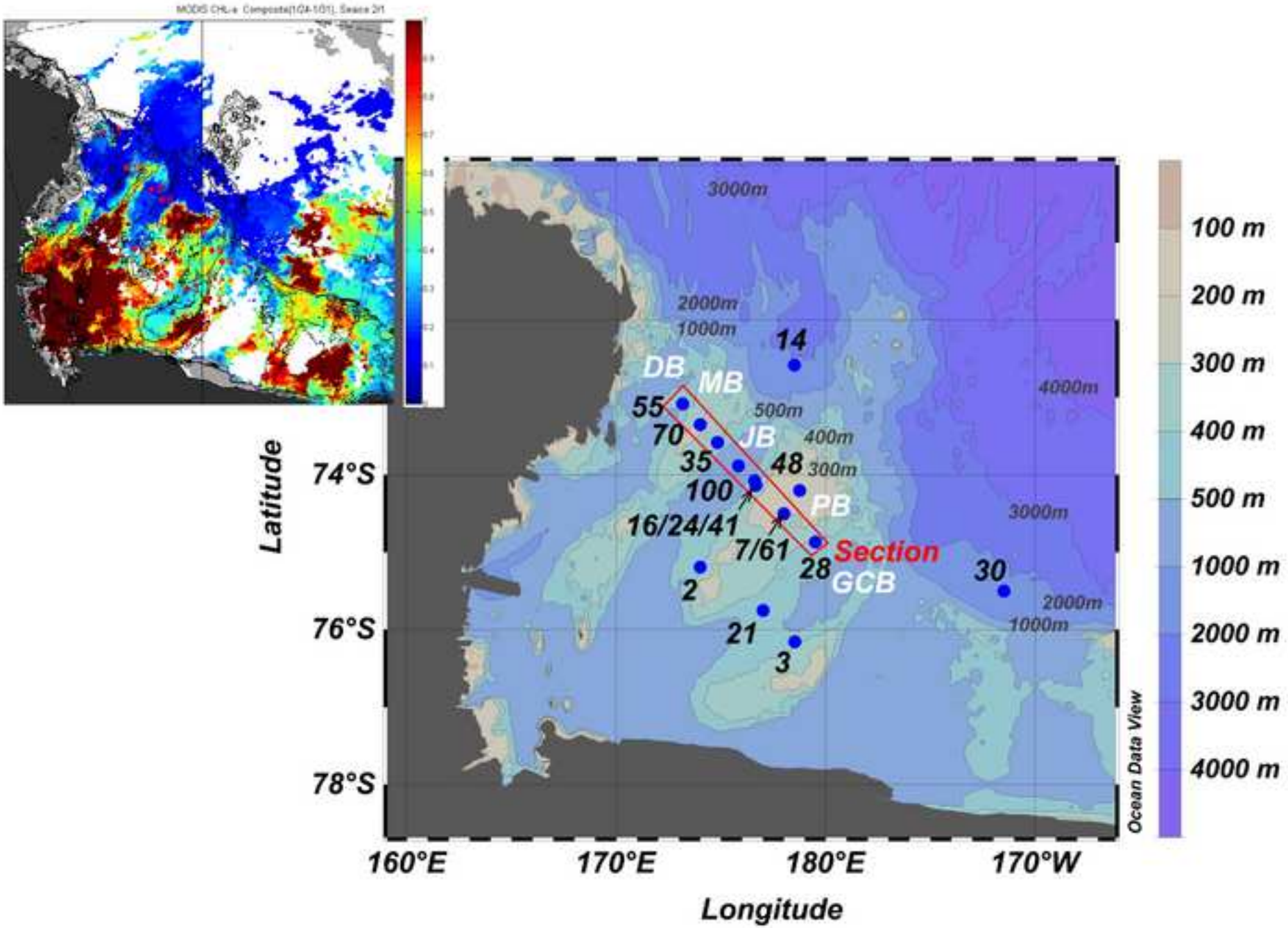

Revised Figure 2_July7

Click here to download high resolution image

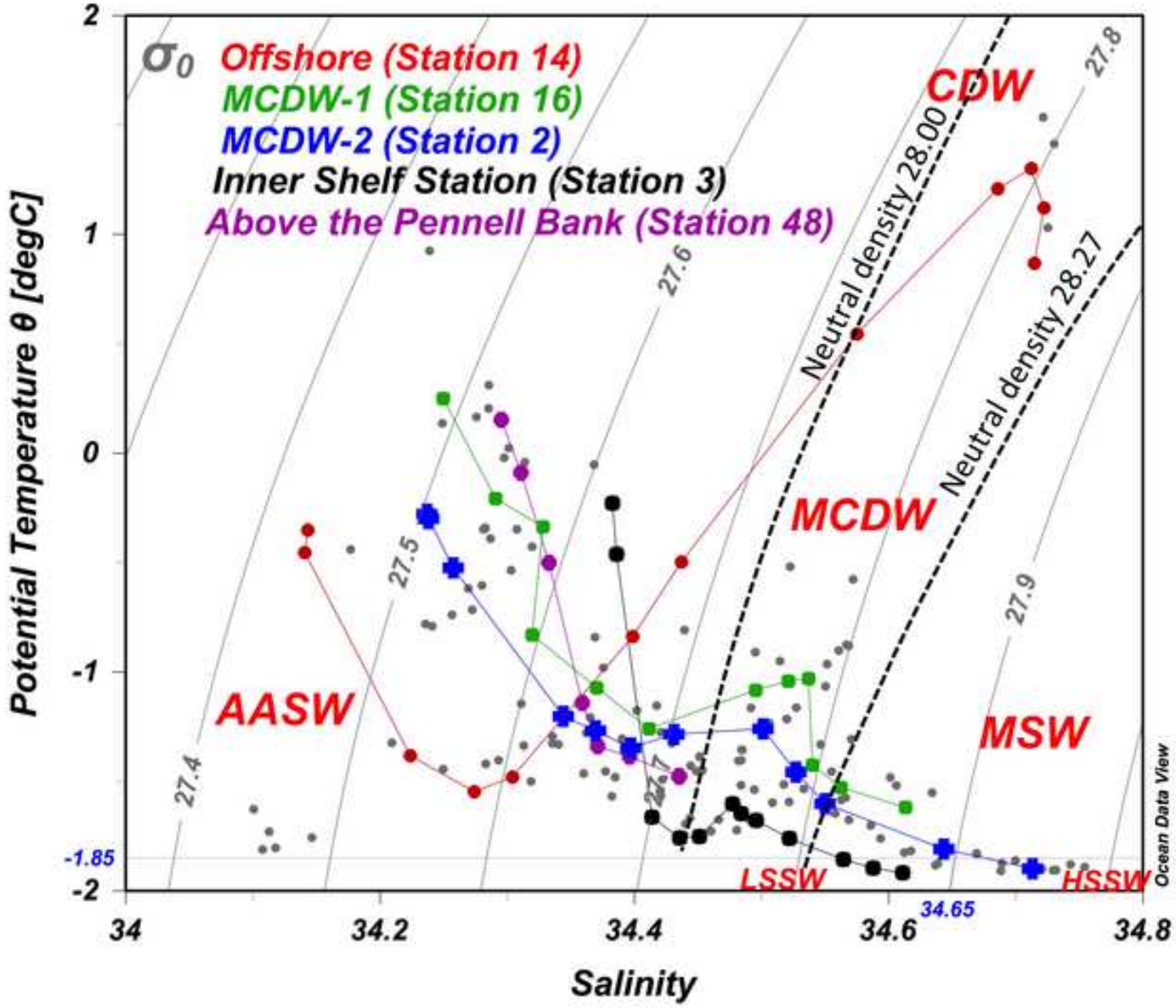

Revised Figure 3

Click here to download high resolution image

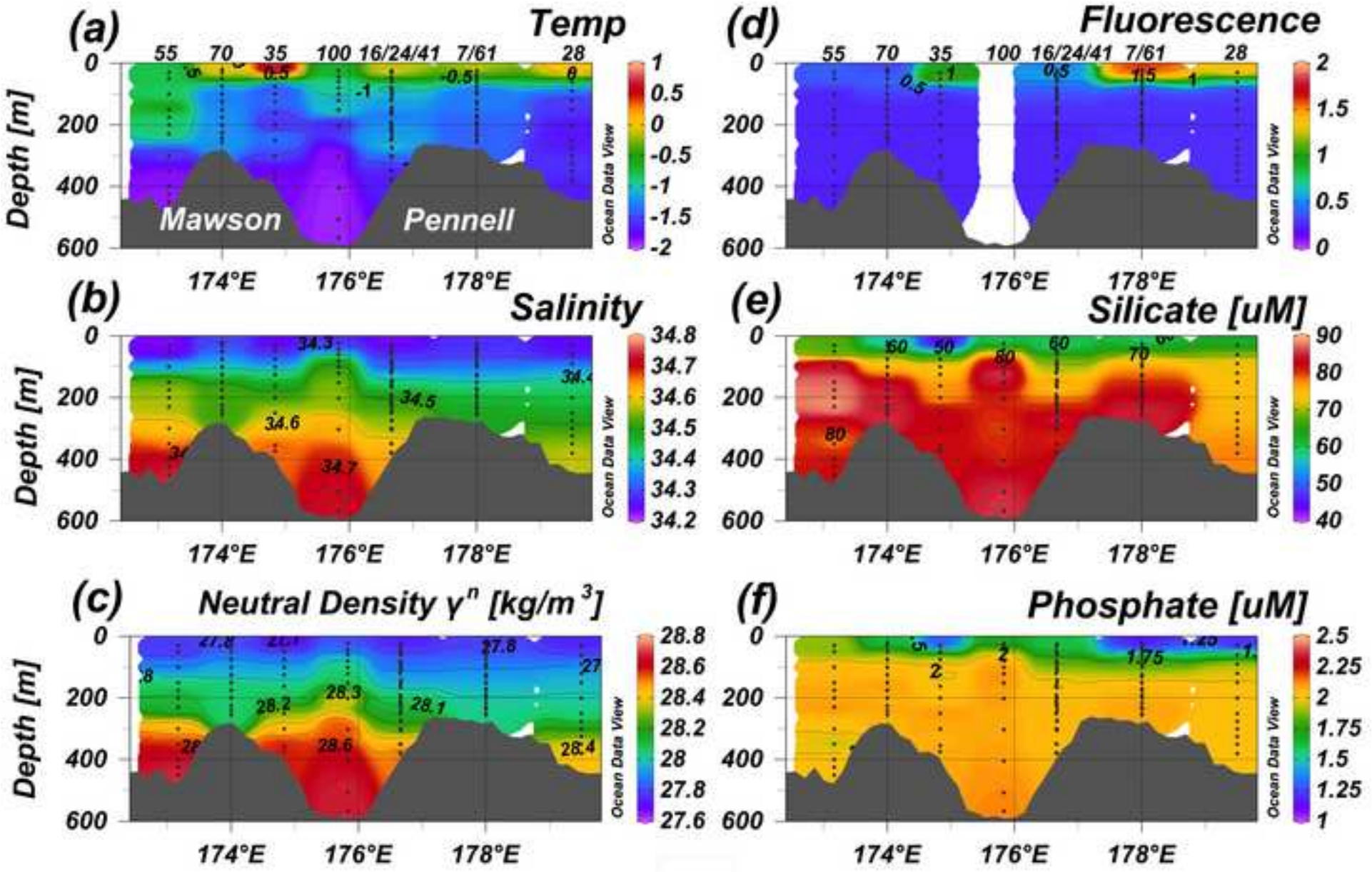

Revised Figure 4

Click here to download high resolution image

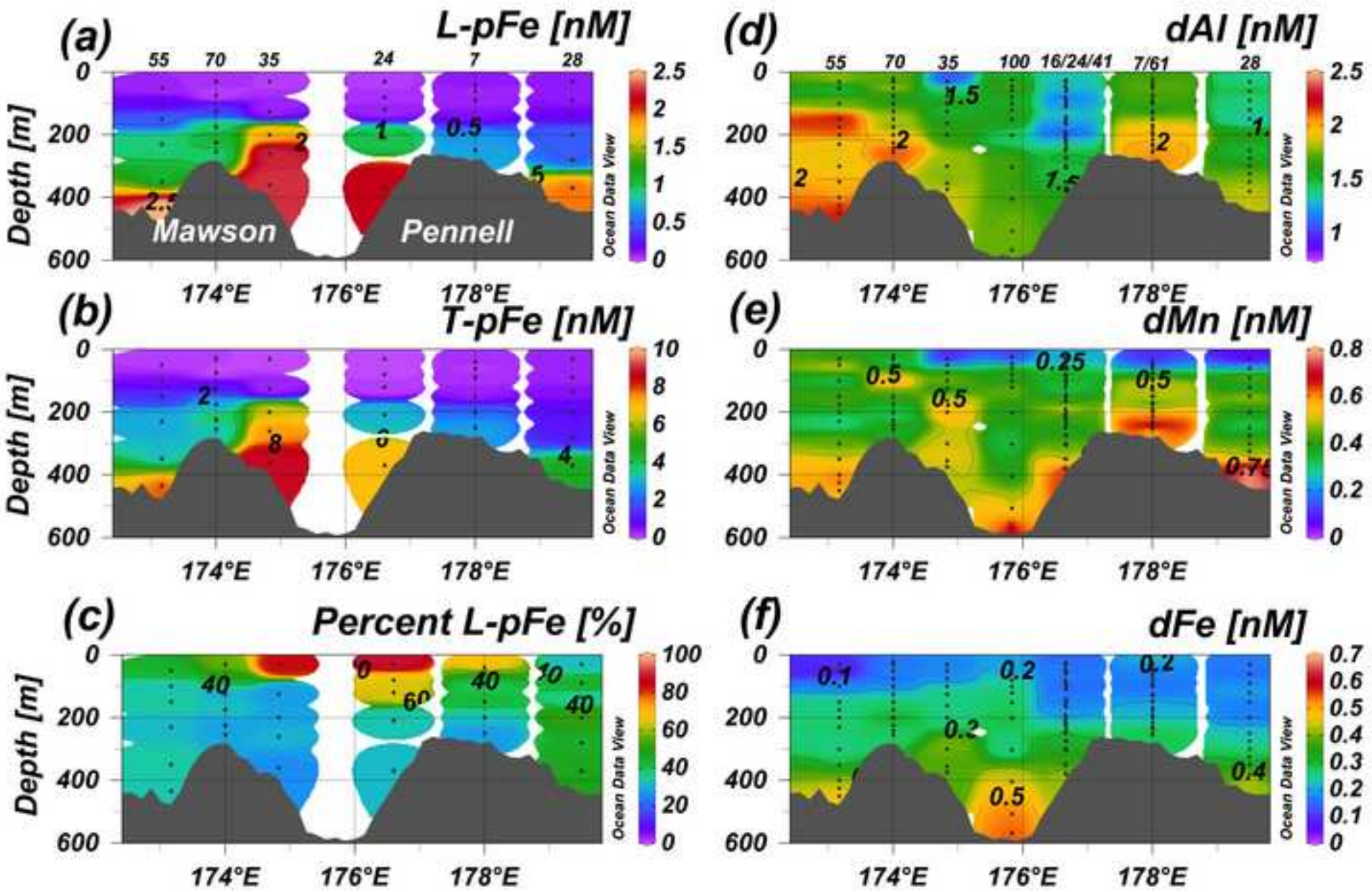

Revised Figure 5

Click here to download high resolution image

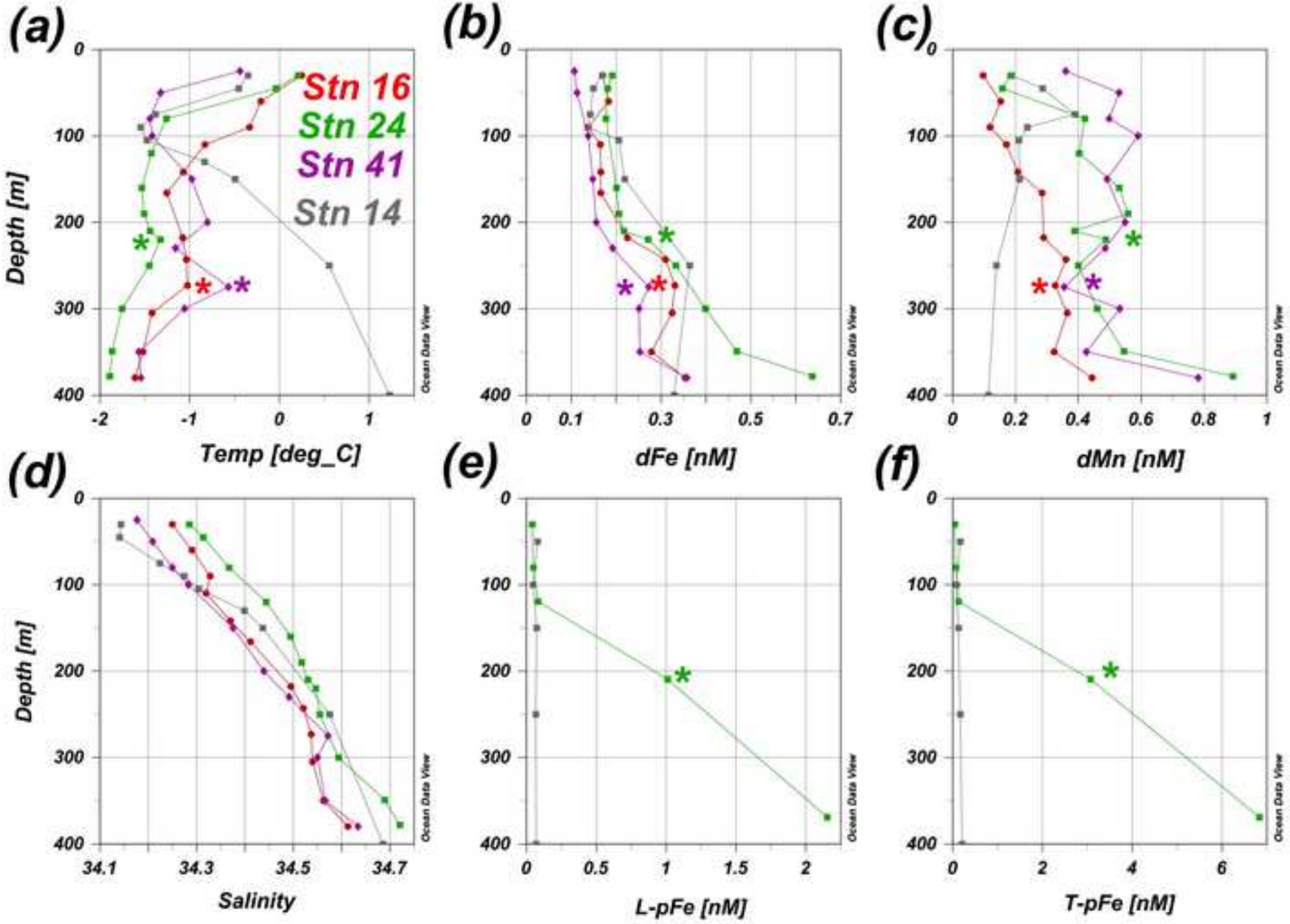

Revised Figure 6

Click here to download high resolution image

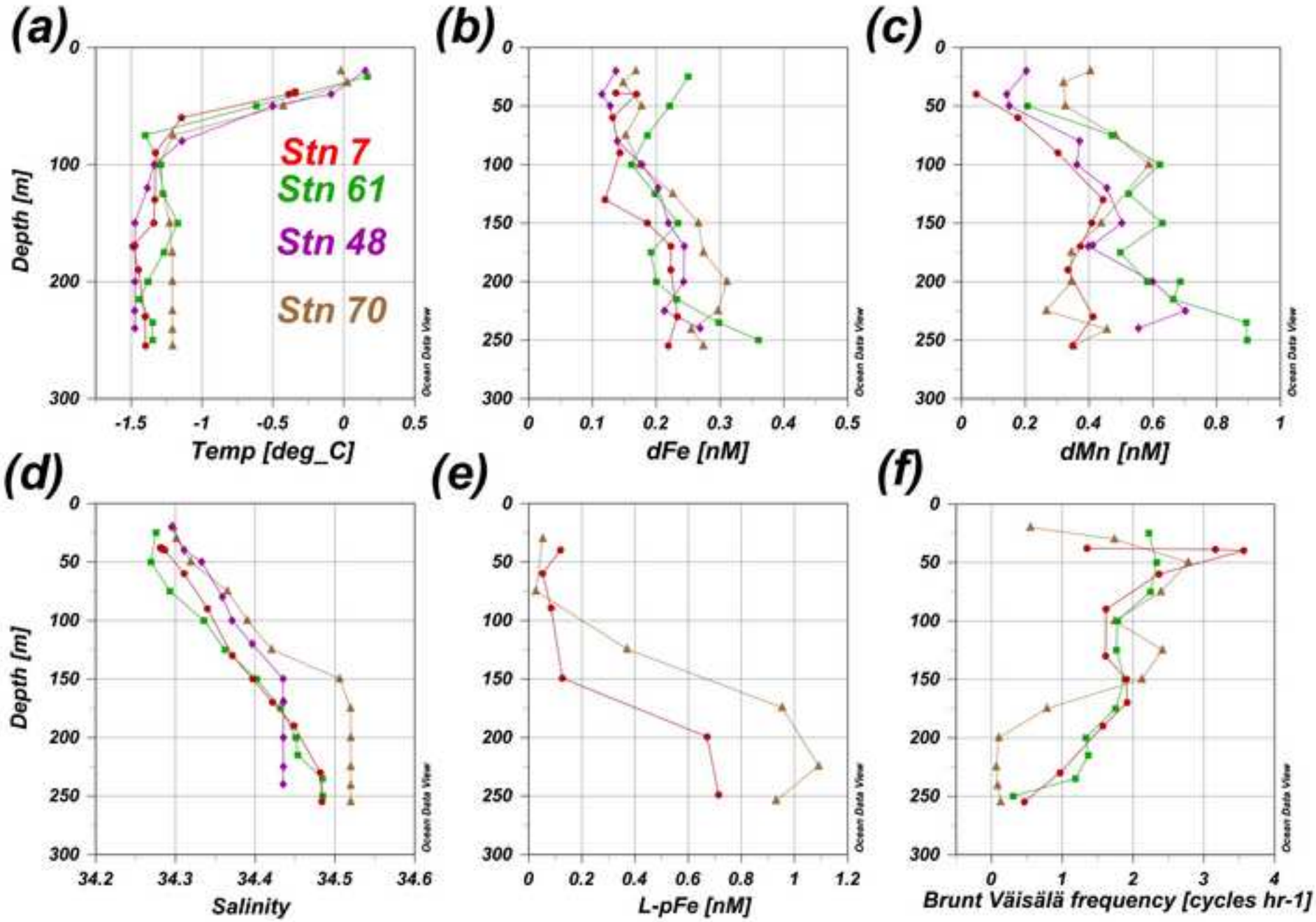

Revised Figure 7

Click here to download high resolution image

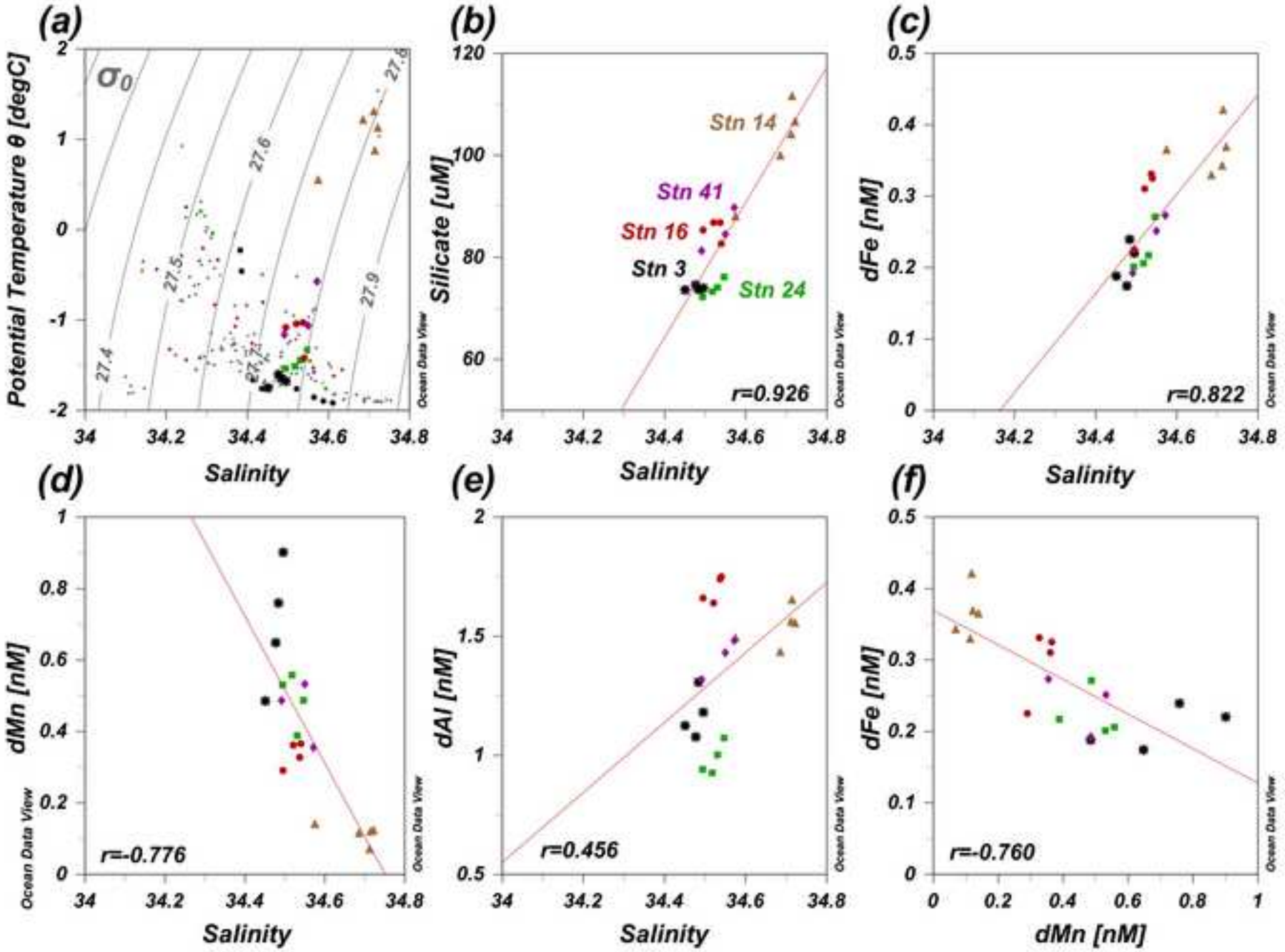

Supplementary material Fig. S1

Click here to download Supplementary material for online publication only: FigS1.jpg

Supplementary material Fig. S2

Click here to download Supplementary material for online publication only: FigS2.jpg

Supplementary material Fig. S3

Click here to download Supplementary material for online publication only: FigS3.jpg

Revised Supplementary material Fig. S4

Click here to download Supplementary material for online publication only: Revised_FigS4_July7.jpg